

Lithostratigraphy, magnetostratigraphy, and radiometric dating of the Stanislaus Group, CA, and age of the Little Walker Caldera

Christopher J. Pluhar^{a*}, Alan L. Deino^b, Nathan M. King^c, Cathy Busby^d,
Brian P. Hausback^e, Tracy Wright^f and Collin Fischer^g

^aEarth and Environmental Sciences Department, California State University, Fresno, CA 93740, USA; ^bBerkeley Geochronology Center, 2455 Ridge Rd, Berkeley, CA 94709, USA; ^c1523 Fountain St, Alameda, CA 94501, USA; ^dDepartment of Earth Science, University of California, Santa Barbara, CA 93101, USA; ^eGeology Department, California State University, Sacramento, CA 95819, USA; ^f1500 Foxridge Road, Geyserville, CA 95441, USA; ^gPO Box 2418, Truckee, CA 96160, USA

(Accepted 25 March 2009)

The Miocene Stanislaus Group (Stanislaus, Calaveras, Tuolumne, Alpine and Mono counties, CA), composed of intercalated latite and quartz-latite (trachyandesite and trachyte/trachydacite) lavas and ignimbrites, provides an important marker for reconstructing the elevation history and tectonic development of the Sierra Nevada and Walker Lane. We present new ⁴⁰Ar/³⁹Ar geochronology and magnetostratigraphy indicating that the Stanislaus Group was emplaced in two pulses: (1) major outpouring of latite lavas at ca. 10.4 Ma and (2) ignimbrite eruptions alternating with lesser lava flow eruptions during ca. 9.4–9.8 Ma. These two events filled the ancestral Stanislaus River drainage in the region of the present Sierra Nevada crest, whereas the ignimbrite eruptions formed the Little Walker Caldera. Our new and previous results date these topographic changes and yield improvements to the Stanislaus Group stratigraphy.

Keywords: Stanislaus Group; palaeomagnetism; Ar/Ar geochronology; Table Mountain Latite; Eureka Valley Tuff, Sierra Nevada

Introduction

As early as the mid-1800s, it was recognized that Tertiary lavas filled an ancestral channel of the Stanislaus River, CA (Figure 1), and preferential erosion of surrounding rocks left inverted topography that records the palaeo-geomorphology and extent of the Miocene river (Trask 1856; Whitney 1865; Ransome 1898; Lindgren 1911). Study of the stratigraphy of these lavas and their associated tuffs (Slemmons 1953, 1966; Al Rawi 1969; Noble *et al.* 1974; Priest 1979; Brem 1984) resulted in the definition of the Stanislaus Group, a regional association of latite (trachyandesite) lavas and quartz-latite (trachytes/trachydacites) ignimbrites that erupted from the vicinity of Sonora Pass, CA. These volcanic rocks filled the ancestral Stanislaus River in places and probably forced the development of a new drainage system, thus leaving a record of the pre-Stanislaus-Group geomorphology, stream gradient, and drainage extent (Figure 1(a,b)). Erosional remnants of these rocks now span a length of 130 km in a WSW–ENE direction, from Knight's Ferry to the Bodie Hills, CA and the Nevada border. This distribution spans much of the

*Corresponding author. Email: cpluhar@csufresno.edu

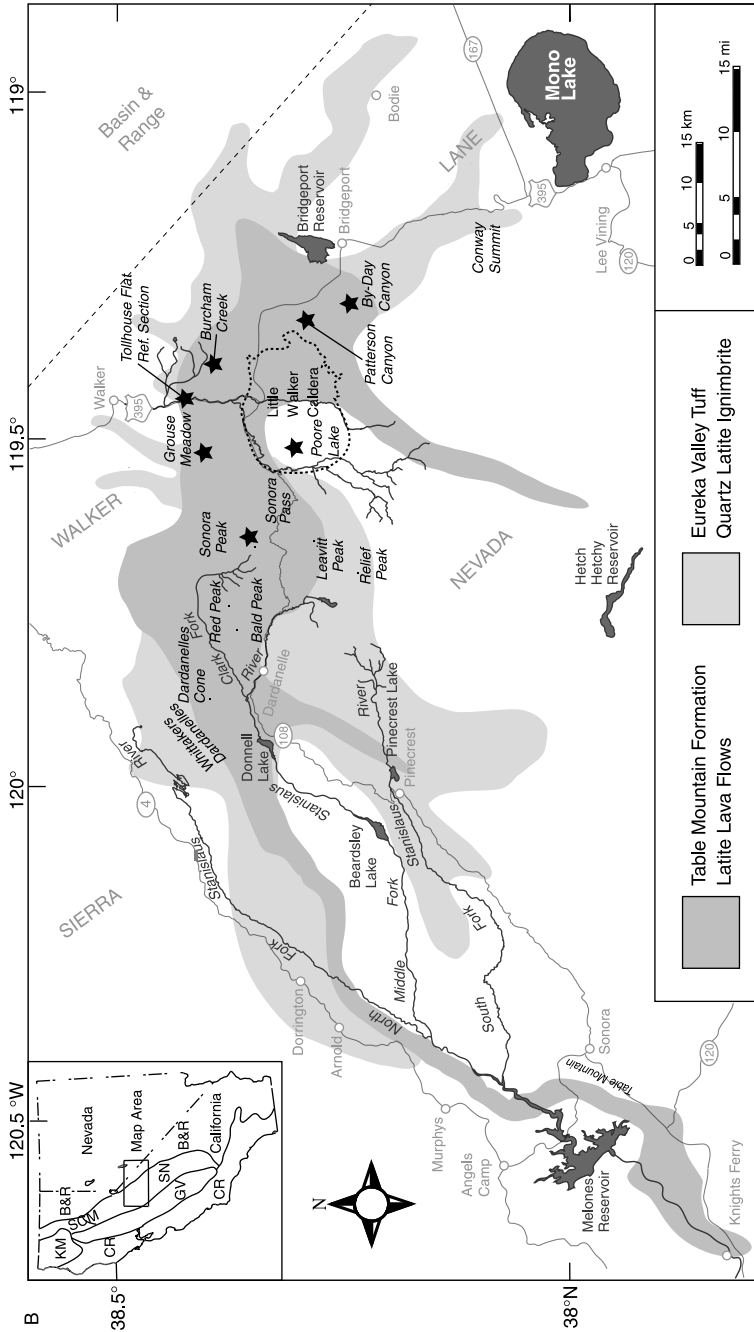


Figure 1. Mapped and interpreted original extent of the Stanislaus Group. (a) Geologic map showing present distribution of Stanislaus Group rocks, the interpreted location of the Little Walker Caldera, and localities referred to in the text (adapted from King *et al.* 2007). (b) Inferred original extent of parts of the Stanislaus Group adapted from Slemmons (1966). The western pattern of the Table Mountain Formation clearly delineates the ancestral Stanislaus River, which is distinct from the present drainage network in the middle and upper elevations of the Sierra Nevada. Outcrops of the Table Mountain Formation near Hetch Hetchy and Pinecrest also indicate that these lavas flowed into adjacent watersheds. The Little Walker Caldera (Priest 1979) bisects the lateral extent of the Stanislaus Group (as interpreted by Slemmons 1966), with the modern Stanislaus River to the west and its inferred pre-Stanislaus-Group headwaters (Bateman and Wahrhaftig 1966; Slemmons 1966) to the east.

rigid Sierra Nevada microplate, and extends across the Walker Lane into the Basin and Range Province. The distinctive Stanislaus Group thus provides both a means of long-distance stratigraphic control and a strain marker for reconstructing tectonic activity within the region (King *et al.* 2007; Busby *et al.* 2008).

Ransome (1898), Lindgren (1911), Bateman and Wahrhaftig (1966), and Wakabayashi and Sawyer (2000, 2001) have used the marked difference between the slope of channel-filling Stanislaus Group rocks and the current Stanislaus River gradient to argue for westward rigid block tilting of the Sierra Nevada since Stanislaus Group emplacement. These and similar studies (Christensen 1966; Huber 1981, 1990) using Neogene channel-filling volcanics of the Sierra Nevada yield estimates of total range crest uplift of between 1490 and 2150 m since about 10 Ma. Unruh (1991) estimated similar uplift magnitude (1900–2400 m) based on the tilt of stratified Cenozoic rocks of the Sierra Nevada Foothills.

During the Oligocene and perhaps early Miocene, ancestral rivers of the Sierra Nevada, including the ancestral Stanislaus, appear to have originated significantly to the east of the current range crest (Lindgren 1911; Bateman and Wahrhaftig 1966; Slemmons 1966; Faulds *et al.* 2005), and subsequent uplift beheaded these streams. It has been proposed that post-mid-Miocene Sierran uplift recorded by the Stanislaus Group was triggered by foundering of a dense eclogite root from the base of the Sierra Nevada (e.g. Ducea and Saleeby 1996, 1998; Manley *et al.* 2000; Farmer *et al.* 2002; Jones *et al.* 2004; Saleeby and Foster 2004), rather than some other trigger (e.g. Chase and Wallace 1988; Small and Anderson 1995). Saleeby *et al.* (2009) presented a model for Neogene Sierran uplift that occurred episodically at ca. 10 and 3.5 Ma due to extensional faulting along the eastern Sierra escarpment and lithospheric delamination, respectively.

This inferred Neogene history of Sierran uplift stands in contrast to data suggesting that the range has been high since it was part of an extensive 'Cretaceous interior Cordillera plateau', with an elevation of at least 3 km (House 2001). Lines of evidence including U–Th/He thermochronology (House *et al.* 1998; House 2001; Cecil *et al.* 2006), hydrogen isotopes recording elevation of palaeoprecipitation (Mulch *et al.* 2006), and palaeobotanical evidence (Wolfe *et al.* 1997) are all consistent with the high-altitude Cordilleran Plateau model. Reconciling these data with evidence for Neogene uplift of the Sierra Nevada is the present subject of intense debate.

The primary goal of the current study is to provide a robust stratigraphy, magnetostratigraphy, and radiometric geochronology for the Stanislaus Group, a principal datum used for reconstructing Neogene Sierran uplift and geomorphology. We present high-precision correlations of Stanislaus Group magnetostratigraphy to the magnetic polarity timescale and integrate this with previous stratigraphic and geochronologic data, permitting stratigraphic correlations to the level of individual lava flows across distances of 100 km or more. The age constraints resulting from this study date stages in the geomorphic evolution of the ancestral Stanislaus River system.

Regional stratigraphy

Cenozoic rocks of the study region lie unconformably upon Palaeozoic/Mesozoic metamorphic rocks intruded by Mesozoic plutonic rocks of the Sierra Nevada batholith. The Cenozoic record in the study area is dominated by four phases of volcanic activity (Slemmons 1953, 1966): (1) rhyolite tuffs and volcanoclastic rocks of the Oligocene to early Miocene Valley Springs Formation, (2) dominantly andesitic tuffs and volcanoclastic rocks of the Miocene Relief Peak Formation (called Mehrten Formation, where

indistinguishable from the Disaster Peak Formation), (3) potassic latite to quartz-latite (trachyandesite to trachyte) lavas and tuffs of the Miocene Stanislaus Group, and (4) dominantly andesitic tuffs and volcaniclastic rocks of the Mio-Pliocene Disaster Peak Formation (called the Mehrten Formation, where indistinguishable from the Relief Peak Formation). Each major phase of volcanic activity is followed by renewed erosion. Much of the volume of each pulse of eruptive material filled or partly filled the existing drainage networks of the time. Re-incision followed each stage of volcanism, leading in some cases to dramatically different stream courses, and preserving some palaeo-drainages as today's interfluves.

Stanislaus Group stratigraphy

Ransome (1898), Slemmons (1953, 1966), Noble *et al.* (1974), and Priest (1979) described the stratigraphy of what is now called the Stanislaus Group with increasing detail, as each worker investigated regions closer to the eruptive source of these rocks (Figure 2). Recent publications typically use the Stanislaus Group stratigraphy of Noble *et al.* (1974) (Figure 2; e.g. King *et al.* 2007; Busby *et al.* 2008). However, Priest (1979) provided the most detailed stratigraphy (Figure 2), having studied the proximal region in and around the Little Walker Caldera. Priest includes nearly all units described by previous workers, but includes additional units and further subdivided some. The present study documents some of Priest's observations, so that a partial review of Priest's stratigraphy (Figure 2) is necessary.

The Table Mountain Formation, the oldest unit in the Stanislaus Group, consists of porphyritic plagioclase, augite, olivine latite lavas, where the labradorite or bytownite plagioclase phenocrysts can be as large as 1–2 cm (Slemmons 1953; Priest 1979). Up to 23 individual lava flows of the Table Mountain Formation are evident at Sonora Peak (Figure 3), for a total thickness exceeding 400 m (Busby *et al.* 2008). Slemmons (1966) placed the eruptive source near Sonora Peak, though Busby (unpublished mapping) finds no evidence for this and prefers a source in the vicinity of the Little Walker Caldera, consistent with Halsey (1953). Table Mountain Formation thins westwards (down palaeocanyon) until it consists largely of a single 48 m-thick palaeocanyon-filling flow in the Sierra Nevada Foothills (Figure 3). In this region at Knight's Ferry (Figure 1), drill coring reveals multiple Table Mountain Latite flows in some locations, which probably represent separate small breakouts from a single main intracanyon flow (Gorny *et al.* 2009).

In the area of the Little Walker Caldera (Figure 1), Priest (1979) informally subdivided the Table Mountain Formation into the Lower Member, Large Plagioclase Member, Two-Pyroxene Member, and Upper Member (Figure 2). Thus far, we have found these subdivisions to be useful only in the vicinity of the Little Walker Caldera and will not apply these names to the Table Mountain Formation outside of the region proximal to the Little Walker Caldera.

Members of the Eureka Valley Tuff (EVT) lie above the Table Mountain Formation. The Tollhouse Flat Member of the EVT overlies the Table Mountain Formation (Figure 2) and consists of voluminous, widespread, densely to moderately welded, quartz-latite ignimbrite. The hallmarks of the Tollhouse Flat Member are: (1) the presence of biotite phenocrysts within the pumice of this member (Noble *et al.* 1974), i.e. not accidental biotite, and (2) reversed palaeomagnetic polarity (Al Rawi 1969; Noble *et al.* 1974). Member thickness, lithic size, and lithic abundance within the Tollhouse Flat Member all decrease away from the Little Walker Caldera, suggesting it as the eruptive source (Priest 1979).

Ransome (1898)	Slemmons (1966)	Noble et al. (1974)	Priest (1979); used in this study unless noted		
Dardanelle Flow	Dardanelles Member	Dardanelles Formation	Lavas of Mahogany Ridge (informal)* Latites of Devil's Gate (informal)*		
	Stanislaus Formation	Stanislaus Group	Stanislaus Group		
				Eureka Valley Tuff	Upper Member /Tuff of Poore Lake
				Eureka Valley Tuff	Fales Hot Spring Quartz Latite*
Biotite - Augite Latite	Eureka Valley Member	Eureka Valley Tuff	By-Day Member		
		Eureka Valley Tuff	Latite within Eureka Valley Tuff - Latite Flow Member**		
		Eureka Valley Tuff	Tollhouse Flat Member		
Table Mountain Flow	Table Mountain Latite Member	Table Mountain Formation	Table Mountain Formation		
			Upper Member*		
			Two Pyroxene Member*		
			Large Plagioclase Member*		
			Lower Member*		

Figure 2. Chart showing evolution of nomenclature of the Stanislaus Group. Priest's (1979) stratigraphic nomenclature is used in this study except that we adopt Brem's (1984) Latite Flow Member of the EVT instead of Priest's 'Latite within the EVT' because it distinguishes between tuff and lava flow. *The position or stratigraphic utility of these units has not yet been independently verified by workers other than Priest (1979). **Name proposed by Brem, adopted here.

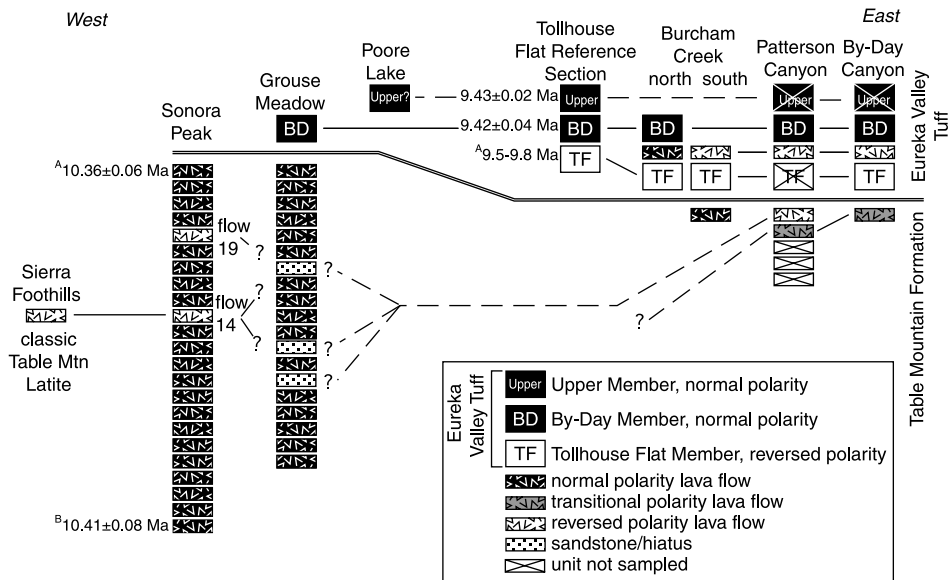


Figure 3. Schematic lithostratigraphy, magnetostratigraphy, and radiometric dating for study localities and regional correlation. Numerical age dates derive from this study unless otherwise noted. Palaeomagnetic remanence results corresponding to each unit are presented in Table 1 with flows being numbered from the bottom of each section. Polarities inferred for the Tollhouse Flat Reference Section and results for Sierra Foothills localities originate from King *et al.* (2007). ^APreferred age from this study is 9.76 ± 0.04 Ma (biotite), but discordance between biotite and plagioclase separates, as well as between different laboratories, yields an age range. ^BAge dates recalculated from Busby *et al.* (2008).

Priest (1979) gives the name 'Latite within the Eureka Valley Tuff' to thin, low-potassium, latite lavas found between the Tollhouse Flat and By-Day members of the EVT in and around the Little Walker Caldera. At Burcham Creek, to the north of the Little Walker Caldera and near Noble's reference section, Brem (1984) corroborated the presence of latite between the Tollhouse Flat and By-Day members, simply calling it 'Latite Flow Member' of the EVT. Slemmons (1953) also mentions a lava flow in this stratigraphic position at the EVT type section in the Bald Peak area, an observation corroborated by Koerner *et al.* (2009).

The By-Day Member of the EVT consists of a voluminous, widespread, densely to moderately welded, quartz-latite ignimbrite. The By-Day Member overlies the Latite Flow Member of the EVT (where it is present) and is normally magnetized (Al Rawi 1969; Noble *et al.* 1974). Unlike the Tollhouse Flat Member, the By-Day Member lacks biotite phenocrysts except for accidental lithics (Noble *et al.* 1974).

The Fales Hot Spring Quartz Latite is a thick, biotite-bearing, quartz-latite lava unit found in a small region within the eastern part of the Little Walker Caldera (Priest 1979). Its age and palaeomagnetic polarity are unknown, though these may be inferred from its stratigraphic position between the upper two members of the EVT.

Noble *et al.*'s (1974) informal Upper Member of the EVT overlies the By-Day Member as well as the Fales Hot Spring Quartz Latite. The Upper Member bears similarity to the Tollhouse Flat Member, exhibiting biotite within its pumice fragments, but differs in its normal polarity magnetization (Noble *et al.* 1974; King *et al.* 2007). In addition, it is areally restricted and distinguishable from the Tollhouse Flat and By-Day members because the Upper Member is, for the most part, non- to poorly welded. To date, it has only been found east of the Sierra crest (Figure 1(a)) and at the Bald Peak type section of the EVT (Koerner *et al.* 2009).

Tuff and lava of Poore Lake is composed predominantly of non- to poorly welded biotite-quartz-latite tuff with minor lavas and dikes (Priest 1979). Tuff of Poore Lake, found in the western part of the Little Walker Caldera, has been tentatively correlated with the Upper Member of the EVT (Priest 1979).

Latites of Devils Gate and Lavas of Mahogany Ridge are localized dikes, plug domes, and lava flows that finish the Stanislaus Group eruptive sequence. These rocks lie within eastern Little Walker Caldera and cut or overlie some of the older units described (e.g. the Upper Member). The diversity of these rocks and the limited geographic extent of any given flow within these groups render these rocks of limited stratigraphic use.

The Dardanelle flow was first named by Ransome (1898) for outcrops near Dardanelle Cone. Elevated to formation status by Noble *et al.* (1974), Dardanelle Formation overlies Ransome's 'biotite-augite latite', now known to be the EVT Tollhouse Flat Member. Until now, Dardanelle had not been documented to overlie the other two members of the EVT. Koerner *et al.* (2009) present evidence that corroborates Noble *et al.*'s (1974) placement of the Dardanelle Formation above the EVT Upper Member.

Prior dating and palaeomagnetic analysis

Initial efforts to date units within the Stanislaus Group used K-Ar methods and generated results spanning ca. 8.8–10.0 Ma (see Noble *et al.* 1974 for a summary). For example, Dalrymple *et al.* (1967) integrated K-Ar age dating with palaeomagnetic polarity results from the Stanislaus Group as part of early attempts at deriving a global magnetic polarity timescale. All K-Ar geochronology on the Stanislaus Group has been superceded by $^{40}\text{Ar}/^{39}\text{Ar}$ geochronology (Busby *et al.* 2008 and that presented here), except for the data

from the Dardanelle Formation. Dalrymple (1964) dated the Dardanelle formation to 9.3 ± 0.4 Ma by K–Ar methods, a result further constrained by its normal polarity, where sampled (King *et al.* 2007). Beck (1960) and Pluhar and Coe (1996) conducted palaeomagnetic analysis on the Table Mountain Formation in the Sierra Foothills, demonstrating that it exhibits a distinctive reversed polarity direction. Al Rawi (1969) conducted magnetic polarity determinations using a portable fluxgate magnetometer as a method of EVT Member correlation across a wide area, providing a magnetostratigraphic framework for studying the EVT.

Busby *et al.* (2008) dated lavas from the Table Mountain Formation and each member of the EVT by the incremental heating $^{40}\text{Ar}/^{39}\text{Ar}$ method. The top and bottom of the Table Mountain Formation at Sonora Peak yielded preferred weighted mean ages of 10.0 ± 0.2 and 10.25 ± 0.06 Ma, respectively, by combining results from whole rock and plagioclase analyses. However, because the whole rock results display recoil spectra and the $(^{40}\text{Ar}/^{36}\text{Ar})_{\text{trapped}}$ component significantly differs from atmospheric composition, we have rejected the whole rock data in favour of the plagioclase results. Plagioclase separates yielded weighted mean plateau ages of 10.14 ± 0.06 and 10.19 ± 0.08 Ma from the top and bottom flows of Table Mountain Formation, respectively. Busby *et al.* (2008) also obtained preferred ages of 9.31 ± 0.03 (weighted mean of plagioclase and biotite), 9.2 ± 0.3 (plagioclase) and 9.15 ± 0.03 Ma (weighted mean of plagioclase and biotite) for the Tollhouse Flat, By-Day, and Upper members, respectively. Converting these ages to the $^{40}\text{Ar}/^{39}\text{Ar}$ monitor age used in this study (see below) yields: (1) 10.36 ± 0.06 and 10.41 ± 0.08 Ma for the top and bottom of the Table Mountain Formation at Sonora Peak, respectively, and (2) 9.51 ± 0.03 , 9.4 ± 0.3 , and 9.35 ± 0.03 Ma for the members of the EVT in ascending order (Renne *et al.* 1998; Kuiper *et al.* 2008). All further references below to ages in Busby *et al.* (2008) will use the revised monitor age.

Palaeomagnetic methods

We collected a total of about 363 oriented core samples for palaeomagnetic analysis through five stratigraphic sections spanning the Stanislaus Group. The Sonora Peak locality lies at the Sierra Nevada crest, while Grouse Meadow, Burcham Creek, Patterson Canyon, and By-Day Canyon localities lie progressively further east of the Sierra Nevada crest and into the Walker Lane Belt (Figure 1). We also collected three oriented hand samples from one unit at Poore Lake. The detailed stratigraphy of the Sonora Peak and Grouse Meadow sections are presented in Busby *et al.* (2008), while schematic stratigraphy of all study localities is summarized in Figure 3.

We collected at least six independently oriented palaeomagnetic samples from the coherent part of each volcanic unit (lava flow or ignimbrite) within each stratigraphic section except in a few cases. Samples were distributed both along (typically across 10+ metres of outcrop, laterally) and through each flow so that unidentified slump blocks, lightning strikes, or baking by subsequent flows would affect at most only one or two samples each. For all lava flow samples, sun compass or sight-point corrections were applied to account for local magnetic anomalies. The samples were subdivided into specimens and then were stepwise demagnetized in an alternating field (AF demagnetization) up to 180 mT. AF demagnetization is our preferred method for removing secondary components from lightning strikes, which commonly affect lavas at high altitudes and mountain tops in this region. Palaeomagnetic analyses were conducted

Table 1. Palaeomagnetic results: Stanislaus Group lava flow and tuff mean directions.

Unit ID	Unit lithology	<i>n</i>	Declination (Geog.)	Inclination (Geog.)	Declination (Strat.)	Inclination (Strat.)	<i>k</i>	α_{95}	ChRM type	Strike	Dip
<i>Sonora Peak</i>											
Flow 23	Tum	8	354.9	57.1	354.9	57.1	222.2	3.8	Mixed	0	0
Flow 22	Tum	6	5.2	56.4	5.2	56.4	410.4	3.6	Mixed	0	0
Flow 21	Tum	7	0.5	60.7	0.5	60.7	88.2	6.5	Fisher	0	0
Flow 20	Tum	8	6.2	60.5	6.2	60.5	71.9	6.7	Mixed	0	0
Flow 19	Tum	7	185.3	-66.2	185.3	-66.2	50.9	9.4	Mixed	0	0
Flow 18	Tum	4	350.7	58.6	350.7	58.6	381.6	4.7	Fisher	0	0
Flow 17	Tum	6	347.3	52.9	347.3	52.9	154.5	5.4	Fisher	0	0
Flow 16	Tum	6	7.3	34.3	7.3	34.3	108.3	6.5	Fisher	0	0
Flow 15	Tum	6	344.8	38.7	344.8	38.7	154.1	5.4	Fisher	0	0
Flow 14	Tum	5	156.8	-24.9	156.8	-24.9	357.7	4.2	Mixed	0	0
Flow 13	Tum	5	15.2	50.7	15.2	50.7	20.1	18.0	Mixed	0	0
Flow 12	Tum	5	25.8	59.3	25.8	59.3	989.6	2.4	Fisher	0	0
Flow 11	Tum	6	346.8	44.1	346.8	44.1	183.6	5.0	Fisher	0	0
Flow 10	Tum	7	339.4	45.5	339.4	45.5	315.7	3.4	Fisher	0	0
Flow 09	Tum	7	15.4	58.6	15.4	58.6	1987.8	1.4	Fisher	0	0
Flow 08	Tum	7	11.7	53.7	11.7	53.7	740.9	2.2	Fisher	0	0
Flow 07	Tum	8	343.0	47.8	343.0	47.8	377.9	3.0	Mixed	0	0
Flow 06	Tum	6	338.9	53.1	338.9	53.1	271.4	4.1	Mixed	0	0
Flow 05	Tum	6	354.6	46.1	354.6	46.1	135.3	5.8	Fisher	0	0
Flow 04	Tum	8	343.8	51.5	343.8	51.5	59.1	7.3	Fisher	0	0
Flow 03	Tum	8	351.7	51.7	351.7	51.7	752.2	2.0	Fisher	0	0
Flow 02	Tum	6	348.4	49.5	348.4	49.5	346.8	3.6	Fisher	0	0
Flow 01	Tum	7	341.0	50.1	341.0	50.1	111.0	5.8	Fisher	0	0
<i>Grouse Meadow</i>											
Unit 17	Tevb	7	42.2	33.9	11.9	43.7	202.7	4.3	Mixed	192.8	37.1
Flow 16	Tum	6	58.6	33.6	26.6	53.3	203.1	5.1	Mixed	192.8	37.1
Flow 15	Tum	5	52.6	41.3	11.4	54.7	91.8	8.3	Mixed	192.8	37.1
Flow 14	Tum	6	64.2	34.4	31.4	57.1	130.3	5.9	Fisher	192.8	37.1
Flow 13	Tum	7	39.0	37.3	6.0	44.0	25.8	12.1	Fisher	192.8	37.1
Flow 12	Tum	6	64.0	33.2	32.8	56.1	87.9	7.5	Mixed	192.8	37.1

Table 1 – continued

Unit ID	Unit lithology	<i>n</i>	Declination (Geog.)	Inclination (Geog.)	Declination (Strat.)	Inclination (Strat.)	<i>k</i>	α_{95}	ChRM type	Strike	Dip
Flow 11	Ttm	6	65.7	41.8	21.9	62.9	389.1	3.4	Fisher	192.8	37.1
Sandstone						Not sampled					
Flow 10	Ttm	6	44.1	41.8	4.5	50.0	90.7	7.1	Fisher	192.8	37.1
Flow 09	Ttm	6	58.7	35.9	23.9	54.9	82.3	7.4	Fisher	192.8	37.1
Flow 08	Ttm	6	47.6	36.7	13.1	48.9	68.1	8.2	Fisher	192.8	37.1
Flow 07	Ttm	5	49.5	33.2	18.6	47.5	152.0	6.2	Fisher	192.8	37.1
Sandstone						Not sampled					
Flow 06	Ttm	6	48.3	27.8	22.9	43.0	131.0	5.9	Fisher	192.8	37.1
Sandstone						Thin, baked – not sampled					
Flow 05	Ttm	6	30.2	47.4	349.2	45.2	384.7	3.4	Fisher	192.8	37.1
Flow 04	Ttm	6	48.0	58.3	340.5	59.5	232.0	4.4	Fisher	192.8	37.1
Flow 03	Ttm	6	37.1	49.6	350.1	50.2	18.2	16.1	Fisher	192.8	37.1
Flow 02	Ttm	4	57.7	32.7	26.7	52.1	230.7	6.1	Fisher	192.8	37.1
Flow 01	Ttm	7	53.3	31.9	23.4	49.0	82.2	6.7	Fisher	192.8	37.1
<i>Poore Lake</i>											
Tuff	Tevu	3	6.5	59.7	43.9	46.0	225.4	8.2	Fisher	360	30
<i>Burcahm Creek Composite Section</i>											
<i>Burcham Creek North</i>											
Unit 06	Tevb	8	6.5	63.0	3.3	49.2	141.6	4.7	Fisher	266	14
Flow 05	Tevl	8	352.4	63.3	353.6	49.3	69.2	6.8	Mixed	266	14
Unit 04	Tevt	11	201.3	-71.9	190.8	-58.6	333.3	2.5	Fisher	266	14
<i>Burcham Creek South</i>											
Flow 03	Tevl	5	218.2	-36.0	216.6	-44.6	8.4	28.7	Mixed	139.3	8.8
Unit 02	Tevt	8	190.0	-52.9	180.9	-59.2	473.4	2.6	Mixed	139.3	8.8
Flow 01	Ttm	10	4.0	61.9	349.2	67.3	226.4	3.2	Mixed	139.3	8.8

Table 1 – continued

Unit ID	Unit lithology	<i>n</i>	Declination (Geog.)	Inclination (Geog.)	Declination (Strat.)	Inclination (Strat.)	<i>k</i>	α_{95}	ChRM type	Strike	Dip
<i>Patterson Canyon</i>											
Unit 06	Tevb	4	2.4	80.6	5.0	52.6	2145.1	2.0	Fisher	276	28
Flow 07	Tevl	6	163.5	-58.9	176.6	-53.9	74.2	7.8	Fisher	320	10
Unit 08	Tevt					Not sampled					
Flow 05	Ttm	6	151.7	-61.2	167.8	-57.8	26.5	13.3	Fisher	320	10
Flow 04	Ttm	7	10.0	-82.5	279.0	-83.6	117.0	5.6	Fisher	320	10
Flow 03	Ttm					Not sampled					
Flow 02	Ttm					Not sampled					
Flow 01	Ttm?					Not sampled					
<i>By-Day Canyon</i>											
Unit 04	Tevb	5	38.6	53.5	22.0	57.3	99.0	7.7	Fisher	192	12
Flow 03	Tevl	4	204.4	-49.3	190.1	-50.4	147.1	8.1	Mixed	192	12
Unit 02	Tevt	7	199.2	-59.2	179.1	-58.6	168.2	4.7	Fisher	192	12
Flow 01	Ttm	9	335.6	-56.8	353.9	-62.4	78.7	5.8	Fisher	192	12

Notes: Tevu, EVT Upper Member; Tevb, EVT By-Day Member – normal polarity and lacking biotite; Tevl, EVT Latite Flow Member; Tevt, EVT Tollhouse Flat Member – reversed polarity and containing biotite; Ttm, Table Mountain Formation.

using the CSU Fresno AGICO JR6 spinner magnetometer or the University of California, Santa Cruz DC-SQUID 2G Enterprises magnetometer housed in a shielded room.

Bedding attitude tilt corrections were applied to sample data assuming original horizontality. The correction for the Grouse Meadow locality was straightforward owing to the presence of intercalated, bedded, lithic sandstones. The corrections for the Burcham Creek and Poore Lake localities were derived from the orientation of eutaxitic textures (fiamme) within the ignimbrite units present. The same method was applied for Patterson and By-Day Canyon localities, but there the wide areal distribution of units made it difficult to ensure that tilt corrections were appropriate for each given site. No tilt correction was applied to the Sonora Peak locality, assuming that the small (several degrees) westward dip of lavas at this locality is dominated by original dip. The assumption of original horizontality may introduce error for sites where lavas were emplaced upon an existing slope as opposed to palaeo-horizontal, or where ignimbrite fabrics were influenced by underlying pre-existing topography (e.g. Chapin and Lowell 1979; Hagstrum and Gans 1989; McIntosh 1991). Hence, some error in remanence directions may result from unrecognized 'initial dip', particularly in the ignimbrites. Where intercalated sediments are absent, estimating the local palaeoslope from the character of a unit's lower contact can help identify or adjust problematic tilt corrections.

Sample demagnetization data were analysed using principal component analysis (Kirschvink 1980; Cogne 2003) to reveal best-fit primary magnetization directions, also called characteristic remanent magnetization (ChRM). For some samples with very large secondary components, the maximum applied AF field was insufficient to fully reveal the ChRM, in which case great circle analysis was applied to the demagnetization paths. Some poorly behaved samples were rejected from further consideration due to multiple strong magnetic overprints, resulting in less than six ChRMs per unit for 10 out of 59 of the studied units (Table 1). Mean directions were calculated for each unit (Fisher 1953; McFadden and McElhinny 1988) from all well-behaved sample ChRMs and/or great circles for that unit.

Radiometric geochronology methods

Incremental-heating $^{40}\text{Ar}/^{39}\text{Ar}$ dating experiments were performed on plagioclase separates from one sample each of the Tollhouse Flat (sample LWC82), By-Day (LWC84) and Upper Member (LWC85) tuffs (Table 2) collected from Noble *et al.*'s (1974) Tollhouse Flat reference section (Figures 1 and 3). Fresh, unaltered biotite was also analysed from the Tollhouse Flat sample, but not from the Upper Member because of evident alteration of the biotite in LWC85.

Mineral separates were prepared by crushing and sieving bulk rock to 40–60 mesh, followed by magnetic separation of phenocrysts, ultrasonic cleaning in distilled water, and handpicking to remove impurities or grains with crystal or melt inclusions. Final separates were loaded into wells in an aluminium disc, interspersed with neutron fluence monitors (Fish Canyon sanidine, reference age 28.201 Ma; Kuiper *et al.* 2008), and irradiated in the TRIGA reactor at Oregon State University in the Cd-lined CLICIT facility for 3 h.

After an interval of radiological cooling, samples were analysed by the $^{40}\text{Ar}/^{39}\text{Ar}$ method at the Berkeley Geochronology Center (BGC). Multi-grain samples (20–40 mg) were degassed in UHV using a 50 W CO_2 laser equipped with a 6 mm integrator lens. Extracted gasses were cleaned of reactive species (CO , NO , etc.) using SAES[®] getters and analysed with an MAP 215-50 mass spectrometer for approximately 20–30 min. Further

details of $^{40}\text{Ar}/^{39}\text{Ar}$ dating procedures at BGC are available in the peer-reviewed literature (Deino and Potts 1990; Deino *et al.* 1990; Best *et al.* 1995; Sharp and Deino 1996).

A total of nine incremental heating experiments were performed. Two to three aliquots of each separate were analysed to check reproducibility. The analytical results are provided in full in this article's associated online version (www.informaworld.com/TIGR).

Palaeomagnetic results and litho/magnetostratigraphic correlations

Palaeomagnetic data were generally straightforward to interpret. The vast majority of sample demagnetization paths were univectorial or exhibited only a slight secondary component that was removed by 10–20 mT (Figure 4). A small minority of samples were heavily overprinted (Figure 4). These samples were a subset of those typically from sites on mountain tops, where lightning strikes are more likely. These samples did not reach stable magnetization directions but usually moved towards expected unit directions. Great circle analysis yielded useful data for most of these overprinted samples. Maximum angular deviation values for sample ChRMs were generally less than 5° . Sample ChRMs and great circles from each lava flow or ignimbrite were typically very well grouped with unit means exhibiting $\alpha_{95} < 10^\circ$ and $k > 50$ (Table 1).

Lava flow or tuff polarity and mean directions are presented in Figure 3 and Table 1, with unit numbering starting at the bottom of each section except: (1) at Patterson Canyon flow 7 and unit 8 (Tollhouse Flat Member) lie below unit 6 (By-Day Member) and (2) Burcham Creek is a composite section with units 2 and 4 being stratigraphically equivalent, as depicted in Figure 3. Figure 5 depicts our directional results and reference directions from King *et al.* (2007) for comparison. Remanence data for the studied rocks are dominantly normal polarity. However, the EVT Tollhouse Flat Member exhibits reversed polarity at all localities sampled and reversed-polarity lavas flow are present at (Figures 3 and 5; Table 1): Sonora Peak flows 14 and 19; Burcham Creek flow 03; Patterson Canyon flows 5 and 7; and By-Day Canyon flow 3. By-Day Canyon flow 1 and Patterson Canyon flow 4 display transitional directions. Note that Priest (1979) identified Patterson Canyon flows 4 (transitional polarity) and 5 (reversed polarity) as 'Lower' and 'Large Plagioclase' members of the Table Mountain Formation, respectively. Future work will investigate whether the polarities of these Table Mountain Formation members are distinctive and permit robust unit correlation between localities. Figure 3 depicts known magnetostratigraphic and lithostratigraphic correlations between localities as well as radiometric age constraints, where relevant.

This study completes preliminary analyses for Sonora Peak and Grouse Meadow sections presented in Busby *et al.* (2008). The Sonora Peak section is mainly composed of normal-polarity latite lavas of the Table Mountain Formation, but contains two reversed polarity zones, each represented by a single lava flow. The lower reversed lava, flow 14, exhibits what we call the 'Classic Table Mountain' remanence direction (Figure 5). This direction was first observed by Beck (1960) in the region of Ransome's original work in the Sierra Nevada Foothills near Sonora, CA, and later formally defined as a reference direction for this unit on the Sierra Nevada microplate by King *et al.* (2007). The upper reversed-polarity lava at Sonora Peak, flow 19, is similar in direction to King *et al.*'s (2007) sites DM 9 and 11 from nearby Leavitt Peak. We tentatively correlate these, with the directional discordance possibly arising from the fact that King *et al.*'s results derived from oriented hand samples originally collected in the 1960s.

At the Grouse Meadow locality (Figure 1), Table Mountain Formation only records normal polarities and is capped by the normal polarity By-Day Member of the EVT.

Table 2. Summary of $^{40}\text{Ar}/^{39}\text{Ar}$ geochronology results.

Run ID	Material	Apparent age plateau				Integrated age (Ma \pm 1 σ)	'Inverse' isochron			
		Age (Ma \pm 1 σ) [†]	MSWD	n/n_{tot}	% ^{39}Ar		Age	MSE	$(^{40}\text{Ar}/^{36}\text{Ar})_t$	MSE
<i>Upper Member of the EVT (LWC85)</i>										
24914-01	PI	9.43 \pm 0.03	1.0	8/8	100.0	9.44 \pm 0.05	\pm 0.04	296	\pm 11	1.1
24914-02	PI	9.44 \pm 0.04	1.6	10/10	100.0	9.41 \pm 0.05	\pm 0.04	275	\pm 19	1.6
		9.43 \pm 0.02				9.43 \pm 0.04	\pm 0.03			
<i>By-Day Member of the EVT (LWC84)</i>										
24912-01	PI	9.33 \pm 0.09	1.6	5/7	90.7	9.0 \pm 0.2	\pm 0.09	294	\pm 2	1.6
24912-02	PI	9.54 \pm 0.16	1.8	6/10	80.1	10.1 \pm 0.2	\pm 0.24	293	\pm 27	2.3
24913-02	PI	9.43 \pm 0.05	1.4	11/12	96.6	9.44 \pm 0.06	\pm 0.09	304	\pm 13	1.9
		9.42 \pm 0.04				9.46 \pm 0.06	\pm 0.06			
<i>Tollhouse Flat Member of EVT (LWC82)</i>										
24923-01	Bi	9.76 \pm 0.05	1.3	11/12	96.7	9.78 \pm 0.1	\pm 0.19	292	\pm 7	1.3
24923-02	Bi	9.75 \pm 0.05	1.7	10/11	95.7	9.78 \pm 0.09	\pm 0.38	285	\pm 14	1.6
		9.76 \pm 0.04				9.78 \pm 0.07	\pm 0.17			
24924-01	PI	9.35 \pm 0.07	1.5	9/10	93.7	9.40 \pm 0.08	\pm 0.26	313	\pm 24	1.5
24924-02	PI	9.35 \pm 0.09	1.9	5/10	68.2	9.60 \pm 0.08	\pm 0.42	281	\pm 37	2.3
		9.35 \pm 0.06				9.50 \pm 0.06	\pm 0.22			
Nucleogenic production ratios										
$(^{36}\text{Ar}/^{37}\text{Ar})_{\text{Ca}}$					$2.65 \pm 0.022 \times 10^{-4}$			$\lambda(^{40}\text{K}_e)/\text{yr}$		$5.81 \pm 0.17 \times 10^{-11}$
$(^{39}\text{Ar}/^{37}\text{Ar})_{\text{Ca}}$					$6.95 \pm 0.092 \times 10^{-4}$			$\lambda(^{40}\text{K}_\beta)/\text{yr}$		$4.962 \pm 0.086 \times 10^{-10}$
$(^{38}\text{Ar}/^{37}\text{Ar})_{\text{Ca}}$					$0.196 \pm 0.0082 \times 10^{-4}$			$\lambda(^{37}\text{Ar})/d$		1.975×10^{-2}
$(^{40}\text{Ar}/^{39}\text{Ar})_{\text{Ca}}$					$7.3 \pm 0.92 \times 10^{-4}$			$\lambda(^{39}\text{Ar})/d$		7.068×10^{-6}
$(^{38}\text{Ar}/^{39}\text{Ar})_{\text{K}}$					$1.22 \pm 0.0027 \times 10^{-2}$			$\lambda(^{36}\text{Cl})/d$		6.308×10^{-9}
$(^{36}\text{Ar}/^{38}\text{Ar})_{\text{K}}$					3.2×10^2			$(^{40}\text{Ar}/^{36}\text{Ar})_{\text{Atm}}$		295.5 ± 0.5
$^{37}\text{Ar}/^{39}\text{Ar}$ to Ca/K					1.96			$(^{40}\text{Ar}/^{38}\text{Ar})_{\text{Atm}}$		1575 ± 2
								$^{40}\text{K}/\text{K}_{\text{Total}}$		0.01167

Notes: Bi, biotite; PI, plagioclase; MSE, the modified standard error, calculated as the standard error multiplied by root MSWD if MSWD > 1; MSWD, the mean square weighted deviation. Weighted mean ages are shown in bold beneath the experiments for each sample or mineral. Boxes indicate preferred age for a sample.

[†] Includes error in J , the neutron fluence parameter.

Nucleogenic production ratios

Isotopic constants and decay rates	
$\lambda(^{40}\text{K}_e)/\text{yr}$	$5.81 \pm 0.17 \times 10^{-11}$
$\lambda(^{40}\text{K}_\beta)/\text{yr}$	$4.962 \pm 0.086 \times 10^{-10}$
$\lambda(^{37}\text{Ar})/d$	1.975×10^{-2}
$\lambda(^{39}\text{Ar})/d$	7.068×10^{-6}
$\lambda(^{36}\text{Cl})/d$	6.308×10^{-9}
$(^{40}\text{Ar}/^{36}\text{Ar})_{\text{Atm}}$	295.5 ± 0.5
$(^{40}\text{Ar}/^{38}\text{Ar})_{\text{Atm}}$	1575 ± 2
$^{40}\text{K}/\text{K}_{\text{Total}}$	0.01167

Notes: Samples were irradiated for 3 h in the Cd-lined, in-core CLICIT facility of the Oregon State University TRIGA reactor. Sanidine from the Fish Canyon Tuff was used as the neutron fluence monitor with a reference age of 28.201 Ma (Kuiper et al. 2008).

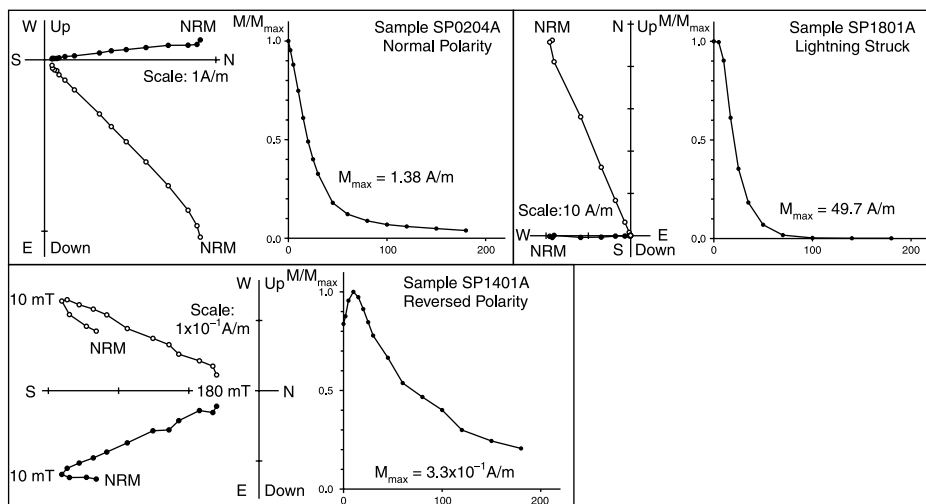


Figure 4. Zijderveld diagrams for selected samples. These representative vector diagrams (Zijderveld 1967) demonstrate the simple behaviour for most of the Stanislaus Group during progressive demagnetization experiments. The sample to the right exhibits a very large secondary overprint, probably from lightning-induced isothermal remanent magnetization, while the samples at the left exhibit very small secondary components followed by univectorial decay towards the origin.

This indicates local hiatuses and/or erosion within the section, resulting in the absence of the reversed latite flows that are present at Sonora Peak. This is corroborated by the presence of bedded sandstones at the Grouse Meadow locality above flows 5, 6, and 10 (Busby *et al.* 2008). In addition, the Tollhouse Flat Member of the EVT is missing from the Grouse Meadow section (Figure 3; Busby *et al.* 2008), although it is present in the next fault block to the west, only a kilometre away (Busby, unpublished mapping). Overall, this indicates that significant portions of the Stanislaus Group are missing from Grouse Meadow.

The composite section at Burcham Creek exhibits EVT Latite Flow Member in stratigraphic context (Figure 3 and Table 1). This locality is composed of two sections on either side of Burcham Creek with the EVT Tollhouse Flat Member in common in both (Burcham Creek units 2 and 4 in Table 1). The southern section at Burcham Creek exhibits one normal-polarity Table Mountain Formation flow at the base, overlain by EVT Tollhouse Flat Member, and capped with a reversed-polarity latite lava. The north side of Burcham Creek exhibits a stratigraphy mapped by Brem (1984): EVT Tollhouse Flat Member at the base, overlain by Latite Flow Member of the EVT, which we find to be normal polarity at this location, and topped with EVT By-Day Member. Thus, the composite section exhibits normal Table Mountain Formation at the base, reversed-polarity EVT Tollhouse Flat Member above that, Latite Flow Member of the EVT of both polarities above that, and is capped by By-Day Member of the EVT. The dual polarity character of EVT Latite Flow Member at Burcham Creek indicates that it was emplaced over a significant period, spanning a magnetic reversal, and we infer that it is composed of at least two localized lava flows. In other words, where it is present, Latite Flow Member of the EVT is composed of one latite lava, but the opposite polarities of the unit on either side of Burcham Creek indicates that it is composed of at least two laterally discontinuous flows.

Lithostratigraphy of the By-Day Canyon section is identical to that of the Burcham Creek composite section: one latite lava flow of Table Mountain Formation at the base,

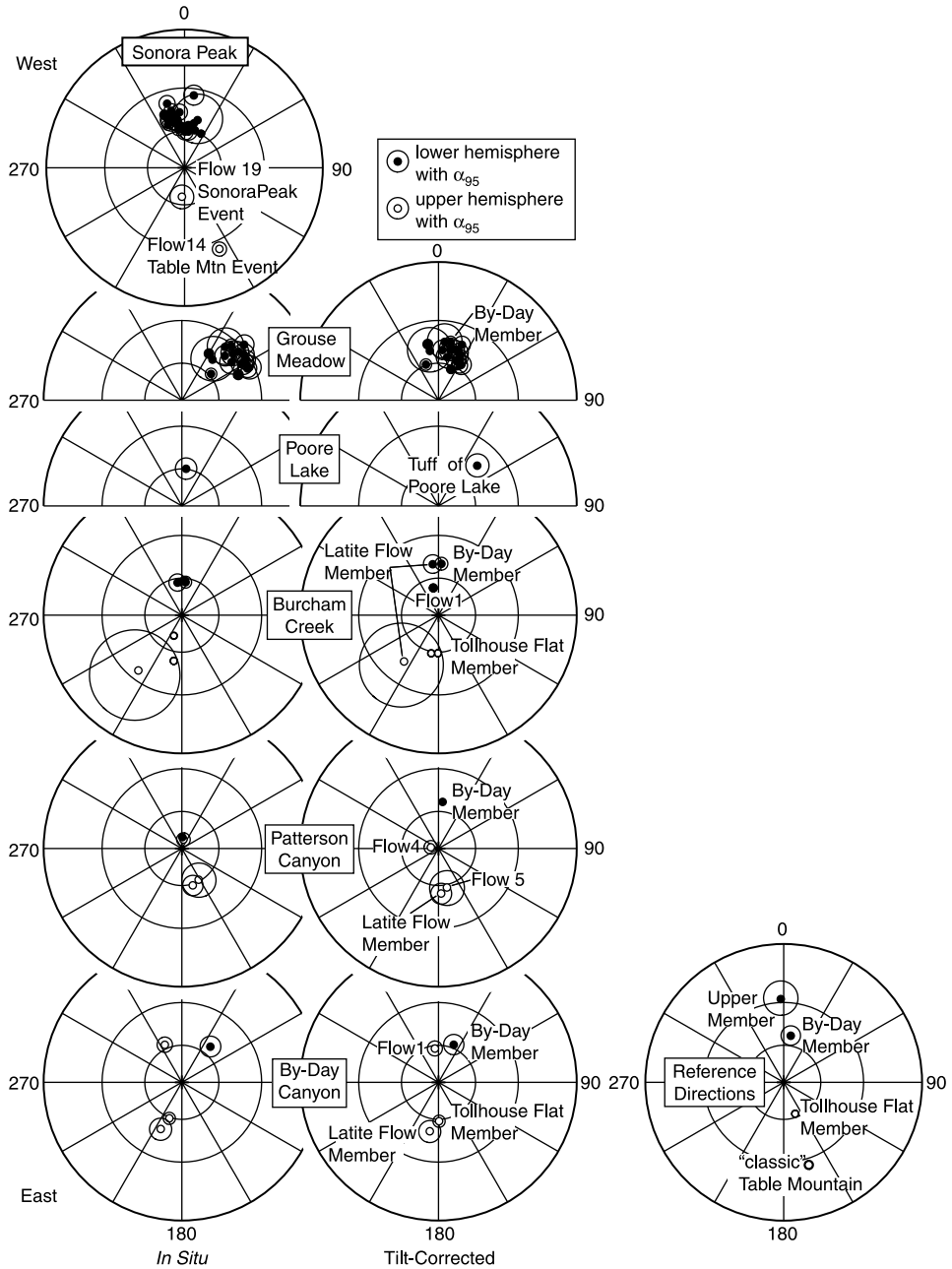


Figure 5. Stereonets depicting flow and tuff mean ChRMs. The mean ChRMs for each unit sampled are depicted with their associated α_{95} 's. Data are grouped by locality. Tilt-corrected data from distinctive units are labelled on the tilt-corrected stereonet. Unlabelled data on the tilt-corrected stereonet derive from the Table Mountain Formation. Reference directions from King *et al.* (2007) are shown for comparison.

overlain by EVT Tollhouse Flat Member, with Latite Flow Member of the EVT above that, and capped by EVT By-Day Member. However, this section differs from Burcham Creek in that the single Table Mountain Formation flow carries transitional, rather than normal polarity (Figure 3). At By-Day Canyon, the Latite Flow Member of the EVT displays reversed polarity. We have not confirmed the existence of EVT Upper Member purported by Priest (1979) to cap this section.

At Patterson Canyon, we sampled a subset of the flows that occur there (Figure 3 and Table 1). Priest's (1979) mapping shows Table Mountain Formation Lower Member (flow 4), with Large Plagioclase Member (flow 5) above that, overlain by the members of the EVT: Tollhouse Flat Member, overlain by Latite Flow Member, and capped by By-Day Member. Priest's mapping (1979) also shows that EVT Upper Member occurs nearby, although stratigraphic continuity is not demonstrated due to the presence of multiple faults crossing the area. Our work demonstrates Table Mountain Formation Lower Member at Patterson Canyon to be of transitional polarity, while Large Plagioclase Member and Latite Flow Member of the EVT display reversed polarity. The flows at the base of this section that we have not sampled are mapped by Priest (1979) as repeated section of Table Mountain Formation Lower Member and Large Plagioclase Member, displaced by faults. Thus far, this explanation of the stratigraphy has not been verified. The remanence directions of the Lower Member (flow 4) and Latite Flow Member of the EVT (flow 7) are each directionally similar to the stratigraphically equivalent latite lavas at By-Day Canyon. The lack of accurate tilt corrections at present for Large Plagioclase Member (Patterson Canyon flow 5) prevents precise directional correlation to reversed flows at Sonora Peak at this time.

Though we did not sample it or verify its presence at either locality, Priest (1979) reported EVT Upper Member at both By-Day and Patterson Canyons. However, within the nearby caldera we did sample Tuff of Poore Lake, which Priest suggested correlates to EVT Upper Member. Three independently oriented hand samples from just east of Poore Lake yield a mean remanence direction that is normal polarity, but significantly different from the two previously published normal-polarity directions for the Upper Member from within the Walker Lane (King *et al.* 2007). This result may be spurious due to alteration, and the accuracy of the remanence direction is also reduced by errors in hand sample orientation and applied tilt corrections derived from eutaxitic tuff textures. Thus, our result for Tuff of Poore Lake does not refute Priest's (1979) tentative correlation of this unit with the Upper Member of EVT. It is broadly consistent with Priest's suggested correlation, within the bounds of current errors and uncertainties of our analysis.

⁴⁰Ar/³⁹Ar geochronology results

Figure 6 shows incremental heating apparent-age spectra for all experiments, and the results are summarized in Table 2. Every experiment yielded an apparent-age plateau, defined as consisting of three or more consecutive steps, comprising more than 50% of the total ³⁹Ar released, that have a mean square weighted deviation (MSWD) indicating the absence of geological error (all scatter in the plateau ages can be attributed to the indicated analytical errors). All plateaus identified in this series of experiments easily meet this criterion, and, in fact, generally encompass more than 90% of the ³⁹Ar release (with two exceptions). Reproducibility of the plateau ages is good; all aliquots of the same separate are statistically indistinguishable (plateau apparent ages are calculated as the weighted mean of included step ages, using inverse variance as the weighting factor). 'Integrated' ages, which are a mathematical isotopic recombination of all steps in an experiment to

estimate the 'total' gas age, are concordant with the plateau ages in all cases. 'Inverse' isochron ages, calculated from a plot of $^{40}\text{Ar}/^{36}\text{Ar}$ versus $^{39}\text{Ar}/^{36}\text{Ar}$, are also concordant with the plateau ages, though because of the narrow spread in isotopic composition and necessity for extrapolation in a significant proportion of the experiments, the errors are much exaggerated compared to the plateau ages. The 'inverse' isochron analysis provides an opportunity to evaluate the $(^{40}\text{Ar}/^{36}\text{Ar})_{\text{trapped}}$ component, which is not significantly different from atmospheric composition (295.5) in all cases. Because the isochron analysis is inappropriate for some samples (e.g. the biotite experiments, where the errors of the isochron ages are exaggerated by a factor of ~ 4 – 8 over the plateau ages), isochron ages are provided for reference but the weighted average of the plateau ages will be used as the preferred age for further geological discussion (Table 2).

Determination of a preferred age for the sample of the Tollhouse Flat Member is complicated by the discordancy of the plateau ages between plagioclase (9.35 ± 0.06 Ma, 1σ error) and biotite (9.76 ± 0.04 Ma). Although the totality of the geological evidence must be considered in assessing whether either mineral yields an accurate age, *a priori* unaltered biotite is the preferred mineral for $^{40}\text{Ar}/^{39}\text{Ar}$ dating over plagioclase, due to its much higher potassium content (~ 0.2 – 1.5% versus 6 – 7% weight %K), hence higher $^{40}\text{Ar}^*$ yield. $^{40}\text{Ar}/^{39}\text{Ar}$ analysis of plagioclase also requires a substantial interference correction from the nucleogenic production of ^{36}Ar from ^{40}Ca , which in the case of sample LWC82 is about 7 – 8% of the age. Biotite requires no substantial nucleogenic isotopic corrections for material of this age. The biotite from sample LWC82 appears fresh. Broad plateaus across virtually the entire ^{39}Ar release spectrum, and the fairly uniform % $^{40}\text{Ar}^*$ content across the biotite experiments, also indicate the absence of significant alteration (Figure 6(A,B)). Integrated ages differ from plateau ages by only a maximum of 0.3% for the biotite, but differ by up to 3% for the plagioclase (aliquot 24924-02 exhibits a substantial upward age shift in the latter 25% of the spectrum that is not part of the plateau). Given these considerations, the biotite mean age of 9.76 ± 0.04 Ma is taken as the preferred age for the Tollhouse Flat Member.

However, prior $^{40}\text{Ar}/^{39}\text{Ar}$ dating of the Tollhouse Flat Member suggests a younger age. Busby *et al.* (2008) obtained concordant weighted mean plateau ages of 9.47 ± 0.04 and 9.54 ± 0.04 Ma for incremental heating experiments on plagioclase and biotite, respectively (ages adjusted for the monitor age used in this study). The plagioclase result is not statistically different from the plagioclase age reported above at the 95% confidence level, but the biotite ages differ significantly. It is difficult to assess the results of the prior dating effort, as full analytical results are not provided, and step-heating spectra show only apparent age against ^{39}Ar release. The spectrum for plagioclase shows a stepping-upward apparent age throughout virtually the entire ^{39}Ar release, whereas the biotite result, with a flat apparent-age plateau, may be more accurate. As there is no ready explanation for the discrepancy between the biotite ages from the two studies, the age of the Tollhouse Flat Member remains equivocal. Although it probably lies in the range 9.8 – 9.5 Ma, further systematic geochronology on multiple samples of this member will be necessary to better evaluate its age.

Preferred results for the By-Day dating experiments are more readily established. Three aliquots of the By-Day plagioclase separate were analysed. Aliquot 24913-02 is best, exhibiting uniform argon release systematics and age until the final $\sim 5\%$ of gas release, for a plateau age of 9.43 ± 0.05 Ma. The other aliquots are less precise and differ from this result by ± 0.1 Ma, although the difference is not statistically significant. A weighted mean of the three plateau ages gives 9.42 ± 0.04 Ma. Busby *et al.* (2008) obtained 9.4 ± 0.3 Ma; the same age but with less precision.

The preferred age for the Upper Member is the weighted mean of two nearly identical incremental-heating experiments with plateaus comprising 100% of the ^{39}Ar release, giving 9.43 ± 0.02 Ma. $^{40}\text{Ar}^*$ is near 100% of the total ^{40}Ar across the majority of the plateau, and Ca/K ratios remain stable until the final 15% of the ^{39}Ar release. The Ca/K ratio of this plagioclase is about six, half, or less than that of the By-Day and Tollhouse Flat plagioclases (12–14), implying overall higher K content, and consequent high $^{40}\text{Ar}^*$ yield and improved precision. Internal evidence of the $^{40}\text{Ar}/^{39}\text{Ar}$ dating systematics indicates that this set of experiments should provide a reasonably robust upper age bound for the EVT. This result is

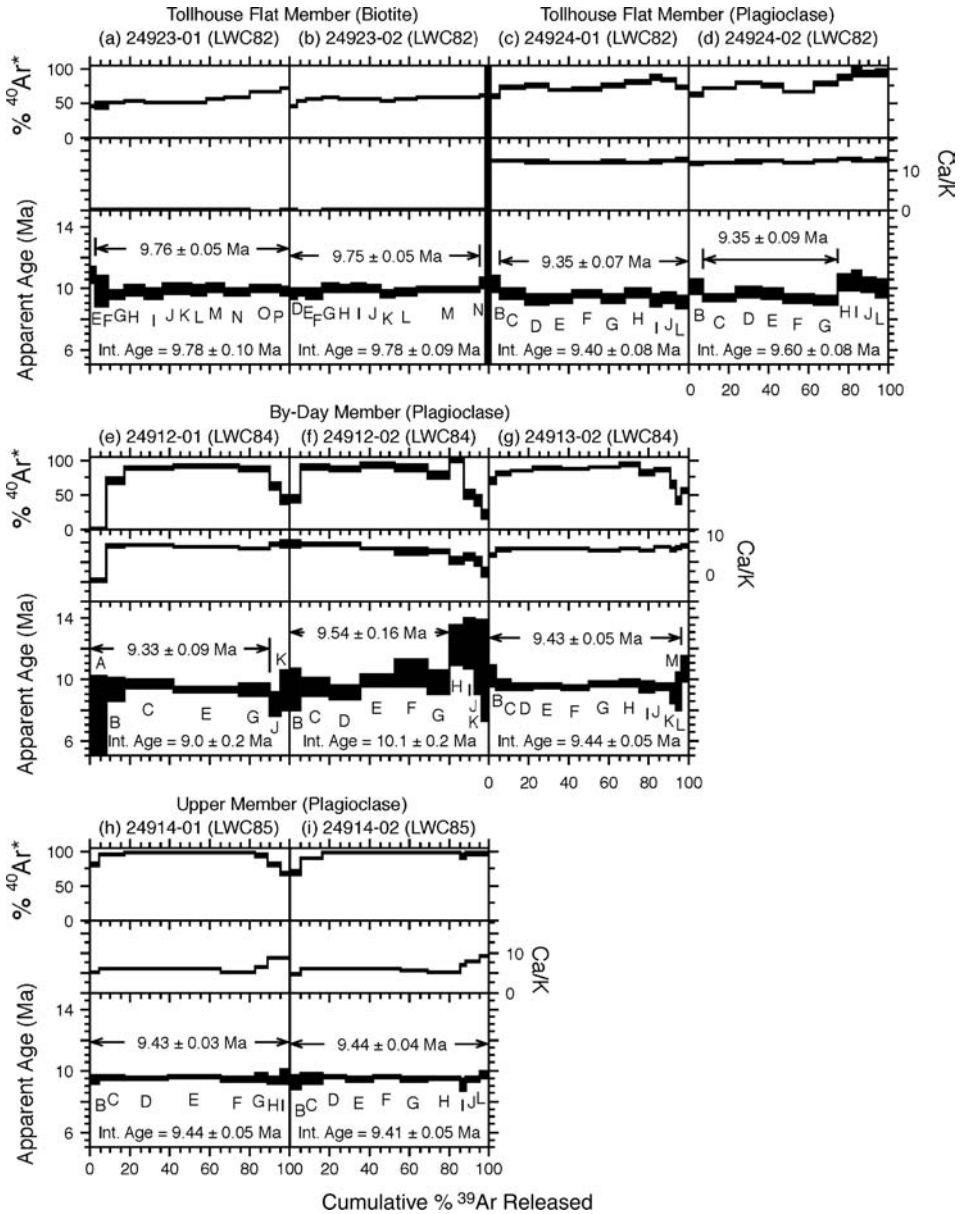


Figure 6. $^{40}\text{Ar}/^{39}\text{Ar}$ geochronology results.

not statistically distinguishable from the prior biotite $^{40}\text{Ar}/^{39}\text{Ar}$ age on this unit of 9.38 ± 0.04 Ma, but is just distinguishable from the prior plagioclase age of 9.34 ± 0.04 Ma (Busby *et al.* 2008). Again, the origin of this discrepancy is not known. As the results of Busby *et al.* (2008) tend to be younger than the results reported herein, there may be a systematic difference in technique, or the disparities could be a function of the samples analysed.

Discussion

Lithostratigraphy and magnetostratigraphy

The Stanislaus Group composite stratigraphy (Figures 2 and 7) is consistent with previously published lithostratigraphy but provides a more complete and detailed integration with palaeomagnetic constraints. Magnetostratigraphy within the Table Mountain Formation provides a means of stratigraphic correlation across a distance of 100 km or more at the level of individual palaeomagnetically distinctive lava flows (Figure 5). This study also verifies the presence of a locally widespread latite lava flow unit between the Tollhouse Flat and By-Day Members of the EVT (Priest 1979; Brem 1984) along the margins of the Little Walker Caldera, for which we retain Brem's nomenclature of 'Latite Flow Member of the EVT'. Higher in the stratigraphic column, palaeomagnetic data for the Tuff of Poore Lake are consistent with eruption around the same time as EVT By-Day and Upper Members (during subchron C4Ar.1n, 9.351–9.443 Ma; Lourens *et al.* 2004). Priest (1979) suggested correlation with the Upper Member. However, at this time, statistical likelihood of correlation between Tuff of Poore Lake and Upper Member cannot be assessed due to large uncertainties resulting from chemical alteration, contributions of errors in tilt corrections, and unit reference direction.

The data presented here provide no insight into the proper placement of Ransome's (1898) Dardanelle Flow (now Formation) into the stratigraphy defined by Priest. However, work by Koerner *et al.* (2009) supports the standard stratigraphic position for the Dardanelle Formation at the top of the Stanislaus Group (Noble *et al.* 1974). This is the same stratigraphic position as Priest's (1979) informal Latites of Devil's Gate or Lavas of Mahogany Ridge. This introduces the possibility that these somewhat-similar units may be identical.

Correlation to the magnetic polarity timescale

A direct comparison can be made between the new $^{40}\text{Ar}/^{39}\text{Ar}$ radiometric ages and the global magnetic polarity timescale. For this, we adapt the currently most-utilized, astronomically calibrated, magnetostratigraphic timescale, ATNTS2004 (Lourens *et al.* 2004) and update the ages of reversals during C4Ar–C5r, based on the work of Evans *et al.* (2007). The $^{40}\text{Ar}/^{39}\text{Ar}$ ages herein are determined using a standard (sanidine of the Fish Canyon Tuff of Colorado) specifically calibrated against an orbitally tuned shallow-marine sequence along the coast of Morocco, which in turn is tied biostratigraphically to the Mediterranean sapropel record (Kuiper *et al.* 2008). Thus, the radiometric ages reported here, and the magnetostratigraphic ages provided in ANTNS2004 and Evans *et al.* (2007), employ a synchronized scale to measure time, clocked by climatic proxy signals forced by perturbations of the Earth's orbit. It must be considered that although magnetozone boundary ages are provided in ATNTS2004 and Evans *et al.* (2007) to the kiloyear level of detail, true accuracy is probably no better than several thousands to tens of thousands of years, due to the major uncertainty regarding delayed lock-in of palaeomagnetic remanence resulting from diagenetic alteration near the sediment–water

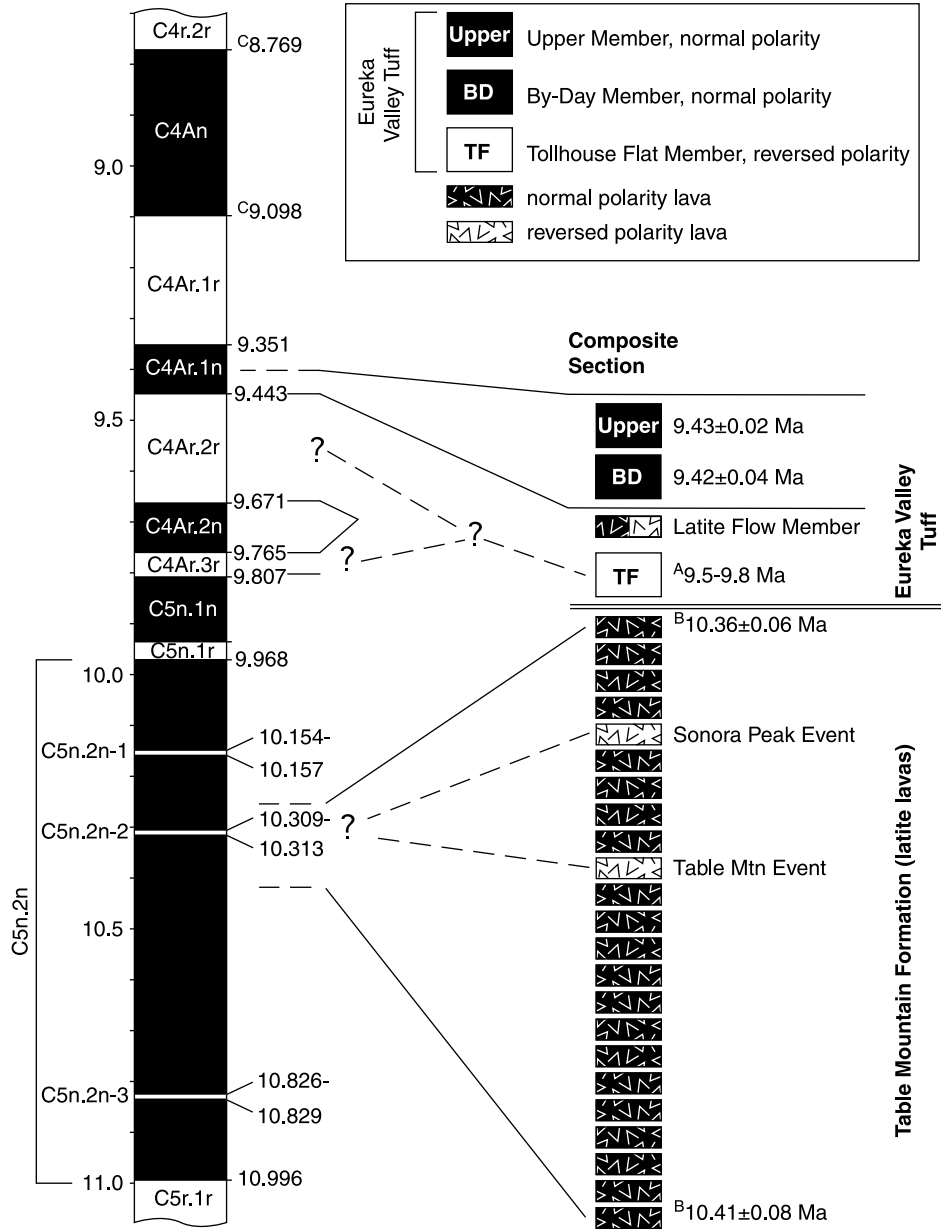


Figure 7. Correlation of the Stanislaus Group composite stratigraphy to the global magnetic polarity timescale. Numerical age dates derive from this study unless otherwise noted. ^APreferred age from this study is 9.76 ± 0.04 Ma (biotite), but discordance between biotite and plagioclase separates, as well as between different laboratories, yields an age range. ^BAge dates recalculated from Busby *et al.* (2008). ^CPolarity reversal age from Lourens *et al.* (2004), while all others derive from Evans *et al.* (2007).

interface in marine sediments (van Hoof 1993). Furthermore, some error in intercalibration of ⁴⁰Ar/³⁹Ar standards and the astronomical timescale may remain.

⁴⁰Ar/³⁹Ar dating of plagioclase separates from the top and bottom of the Table Mountain Formation at Sonora Peak, 10.36 ± 0.06 and 10.41 ± 0.08 Ma, respectively,

(recalculated from Busby *et al.* 2008) places these lavas within normal chron C5n.2n (9.968–10.996 Ma). The Sonora Peak magnetostratigraphy exhibits two reversed magnetozones (represented by one lava flow each), while Evans *et al.* (2007) display only one reversed subchron, C5n.2n – 2 (10.309–10.313 Ma), that satisfies the age dating. Two hypotheses could explain the available data: (1) the Sonora Peak lavas recorded polarity fluctuations during this interval that were not faithfully recorded in sediments used to develop the Evans age model, or (2) there is a systematic age difference between the Evans *et al.* (2007) results during this time interval and the astronomically tuned Fish Canyon Sandstone age. Until these reversed lava flows can be correlated with the global magnetic polarity timescale, we informally dub Sonora Peak flow 14 as the Table Mountain Event, since this flow forms the distinctive Table Mountain at Sonora, CA, while Sonora Peak flow 19 is informally named the Sonora Peak Event.

The $^{40}\text{Ar}/^{39}\text{Ar}$ preferred age for the EVT Tollhouse Flat Member is here determined to be 9.76 ± 0.04 Ma and exhibits reversed palaeomagnetic polarity. This observed age and polarity would place the Tollhouse Flat Member near the beginning of the short subchron C4Ar.3r (9.807–9.765 Ma). Alternatively, using the age recalculated from Busby *et al.* (2008) for this member of 9.51 ± 0.03 Ma, the tuff falls within the middle of the next higher reversed interval, subchron C4Ar.3r (9.671–9.443 Ma). The By-Day Member has normal palaeomagnetic polarity and an $^{40}\text{Ar}/^{39}\text{Ar}$ age of 9.42 ± 0.04 Ma, while the normal-polarity Upper Member has an $^{40}\text{Ar}/^{39}\text{Ar}$ age from this study of 9.43 ± 0.02 Ma. These dates place both of these normal polarity EVT members, just above the lower boundary of normal subchron C4Ar.1n (9.443–9.351 Ma), in excellent agreement with the magnetic polarity timescale.

Implications for evolution of the ancestral Stanislaus River

Priest (1979) reported lacustrine sediments within the Little Walker Caldera, resulting from internal drainage into the post-collapse depression. Results presented here constrain the EVT eruption and associated formation of the Little Walker Caldera to a short period during 9.4–9.8 Ma. In addition, the gap in age between the ca. 10.4 Ma Table Mountain Formation at Sonora Peak and the regionally traceable EVT requires a local unconformity (hiatus or erosion) spanning 0.6–1.0 million years. Given the dominant normal polarity of the Table Mountain Formation, wherever it has been sampled, the local unconformity at Sonora Peak probably reflects a real cessation or major slowdown in eruptive activity between these formations.

Emplacement of the Stanislaus Group had major implications for the local topography and drainage network. Based on clast lithologies in the Pre-Stanislaus-Group gravels and the outcrop pattern of the Stanislaus Group, Bateman and Wahrhaftig (1966) and Slemmons (1966) suggested that the ancestral Stanislaus River sourced substantially to the east of the current Sierra crest and Little Walker Caldera. However, the Table Mountain blanket of lavas exceeded 400 m near the present Sierra crest (Busby *et al.* 2008) and may have filled the drainage system there to overflowing, forming a nearly continuous sheet just west of the Little Walker Caldera. This is suggested by two observations: (1) the highest peaks at the Sierra crest (e.g. Leavitt and Sonora Peaks) are capped by the Table Mountain Formation, and (2) Table Mountain Formation flowed into at least three distinct drainages (Slemmons 1966; Huber 1990), two separate forks of the ancestral Stanislaus River and the ancestral Tuolumne River, as evidenced by an outcrop pattern that diverges down palaeoslope (Figure 1(b)). After Table Mountain Formation emplacement at ca. 10.4 Ma, a hiatus of 0.6–1.0 million years probably permitted some re-establishment of a

drainage network. This network was choked by the eruption of the EVT at ca. 9.4–9.8 Ma, at the same time that Little Walker Caldera collapse created an internally drained basin (Priest 1979).

One visible result of these events was the establishment of a post-Stanislaus-Group drainage network that did not follow the former channels filled by these volcanics, except at the edge of the Great Valley (Figure 1(a,b)). Former channels, now preserved by the Table Mountain Formation, form present-day interfluves in the middle elevations of the Sierra Nevada east of 120.2° W longitude. It is not known whether the fluvial reorganization immediately postdated Stanislaus Group emplacement, or was progressive during Disaster Peak Formation emplacement as well. Little Walker Caldera Formation may have further disrupted the drainage system in the region, as it bisects the inferred former extent of the ancestral Stanislaus River (Figure 1(b)). However, it is difficult to separate this effect from that of Sierra Nevada range front faulting, for which there is extensive evidence and which had begun in this area by Stanislaus Group time (Putirka and Busby 2007; Busby *et al.* 2008; Busby and Putirka 2009).

Conclusions

New $^{40}\text{Ar}/^{39}\text{Ar}$ geochronology of the EVT at the Noble *et al.* (1974) reference section yields preferred ages of: (1) 9.76 ± 0.04 Ma for the Tollhouse Flat Member, (2) 9.42 ± 0.04 Ma for the overlying By-Day Member, and (3) 9.43 ± 0.02 Ma for the Upper Member. Combined with palaeomagnetic results, this constrains the By-Day and Upper Members to chron C4Ar.1n (9.351–9.443 Ma). The present and previous reported age data for the Tollhouse Flat Member are discordant. However, radiometric and magnetostratigraphic results together constrain the Tollhouse Flat Member eruption to chrons C4Ar.2r (9.443–9.671 Ma) or C4Ar.3r (9.765–9.807 Ma). Earlier radiometric dating indicates that the Table Mountain Formation was emplaced around 10.4 Ma. Thus, the Stanislaus Group spans almost a million years, but was emplaced episodically during ca. 9.4–9.8 and 10.4 Ma.

Several improvements to stratigraphic control result from the current study. The magnetostratigraphy of the Table Mountain Formation exhibits two separate reversed-polarity latite lava flows nested within at least 21 normal-polarity flows that formed during chron C5n.2n (9.968–10.996 Ma). $^{40}\text{Ar}/^{39}\text{Ar}$ geochronologic constraints from prior work indicate that these two separate reversed subchrons occurred around the time of C5n.2n – 2 (10.309–10.313 Ma). The absence of two reversed subchrons of this age in the polarity timescale suggests that the Table Mountain Formation may record events absent from or averaged out of ocean sediment cores used to develop the polarity timescale used here (Evans *et al.* 2007). The palaeomagnetic distinctiveness of these reversed flows within the Table Mountain Formation, informally dubbed the Sonora Peak Event and the Table Mountain Event, introduces the possibility of widespread stratigraphic correlation using these ‘marker’ beds. This adds to the stratigraphic control within the Stanislaus Group already afforded by the EVT Tollhouse Flat and By-Day Members. We verify the presence of the Latite Flow Member between the Tollhouse Flat and By-Day Members of the EVT. The Latite Flow Member is composed of low-potassium latite (Priest 1979) of both normal and reversed polarities. Magnetic polarity data are consistent with Priest’s (1979) tentative correlation of the Tuff of Poore Lake with the Upper Member of the EVT, but unresolved remanence directional differences between these units leave precise correlation uncertain.

From the reported age constraints, we have precisely dated: (1) the filling by the Table Mountain Formation of the ancestral Stanislaus River in the region of Sonora Peak to ca. 10.4 Ma, and (2) the formation of the Little Walker Caldera to 9.4–9.8 Ma. Reorganization of the fluvial network east of about 120.2° W longitude after this time suggests emplacement of these rocks as a possible cause. Formation of the Little Walker Caldera had unknown effects on the ancestral Stanislaus River system.

Acknowledgements

The authors gratefully acknowledge peer reviewers Jonathan M.G. Glen and John Wakabayashi. Early versions of the manuscript benefited greatly from review by Kellie Townsend. We are also indebted to the following individuals for assistance in the field: Nick Jarboe, Keith Putirka, Rohit Sharma, Kellie Townsend, Robin Trayler, Nitin Vaid, and Singleton Yost. Many thanks to Robert S. Coe for use of the UC Santa Cruz Palaeomagnetism Laboratory. Financial support for stratigraphic, structural, and palaeomagnetic sampling at Sonora Peak and Grouse Meadows was provided in part by NSF EAR- 0711276 (to Putirka and Busby) and EAR- 0711181 (to Busby).

References

- Al Rawi, Y.T., 1969, Cenozoic history of the northern part of Mono Basin (Mono county): CA, NV: University of California at Berkeley, 188 p.
- Bateman, P.C., and Wahrhaftig, C., 1966, Geology of the Sierra Nevada: Bulletin, California: Division of Mines and Geology, v. 190, p. 107–172.
- Beck, M.E., 1960, Paleomagnetism of the Table Mountain Latite, Alpine, Tuolumne, and Stanislaus counties: CA: Stanford University.
- Best, M.G., Christiansen, E.H., Deino, A.L., Gromme, C.S., and Tingey, D.G., 1995, Correlation and emplacement of a large, zoned, discontinuously exposed ash flow sheet; the (super 40) Ar/(super 39) Ar chronology, paleomagnetism, and petrology of the Pahranaagat Formation, Nevada: Journal of Geophysical Research, v. 100, no. 12, p. 24,593–24,609.
- Brem, G.F., 1984, Geologic map of the Sweetwater Roadless Area, Mono County, California, and Lyon and Douglas counties, Nevada: Reston, VA: US Geological Survey.
- Busby, C.J., Hagan, J.C., Putirka, K., Pluhar, C.J., Gans, P.B., Wagner, D.L., Rood, D., DeOreo, S.B., and Skilling, I., 2008, The ancestral Cascades Arc; Cenozoic evolution of the central Sierra Nevada (California) and the birth of the new plate boundary: Special Paper – Geological Society of America. Boulder, CO: Geological Society of America (GSA), p. 331–378.
- Busby, C.J., and Putirka, K., 2009, Miocene evolution of the western edge of the Nevadaplano in the central and northern Sierra Nevada: palaeocanyons, magmatism, and structure: International Geology Review, v. 51, p. 670–701.
- Cecil, M.R., Ducea, M.N., Reiners, P.W., and Chase, C.G., 2006, Cenozoic exhumation of the northern Sierra Nevada, California, from (U–Th)/He thermochronology: Geological Society of America Bulletin, v. 118, no. 11, p. 1481–1488.
- Chapin, C.E., and Lowell, G.R., 1979, Primary and secondary flow structures in ash-flow tuffs of the Gribbles Run paleovalley, central Colorado: Special Paper – Geological Society of America. Boulder, CO: Geological Society of America (GSA), p. 137–154.
- Chase, C.G., and Wallace, T.C., 1988, Flexural isostasy and uplift of the Sierra Nevada of California: Journal of Geophysical Research, v. 93, no. B4, p. 2795–2802.
- Christensen, M.N., 1966, Late Cenozoic crustal movements in the Sierra Nevada of California: Geological Society of America Bulletin, v. 77, no. 2, p. 163–181.
- Cogne, J.P., 2003, PaleoMac; a Macintosh (super TM) application for treating paleomagnetic data and making plate reconstructions: Geochemistry, Geophysics, Geosystems – G [super 3], v. 4, no. 1, p. 23.
- Dalrymple, G.B., 1964, Cenozoic chronology of the Sierra Nevada, California, University of California Publications in Geological Sciences: Berkeley, CA: University of California, 41 p.
- Dalrymple, G.B., Cox, A., Doell, R.R., and Gromme, C.S., 1967, Pliocene geomagnetic polarity epochs: Earth and Planetary Science Letters, v. 2, no. 3, p. 163–173.
- Deino, A.L., and Potts, R., 1990, Single-crystal ⁴⁰Ar/³⁹Ar dating of the Ologresailie Formation, southern Kenya Rift: Journal of Geophysical Research, v. 95, no. B6, p. 8453–8470.

- Deino, A.L., Tauxe, L., Monaghan, M., and Drake, R., 1990, $^{40}\text{Ar}/^{39}\text{Ar}$ age calibration of the litho- and paleomagnetic stratigraphies of the Ngorora Formation, Kenya: *Journal of Geology*, v. 98, no. 4, p. 567–587.
- Ducea, M.N., and Saleeby, J.B., 1996, Buoyancy sources for a large, unrooted mountain range, the Sierra Nevada, California; evidence from xenolith thermobarometry: *Journal of Geophysical Research*, v. 101, no. B4, p. 8229–8244.
- Ducea, M., and Saleeby, J.B., 1998, A case for delamination of the deep batholithic crust beneath the Sierra Nevada, California: *International Geology Review*, v. 40, no. 1, p. 78–93.
- Evans, H.F., Westerhold, T., Paulsen, H., and Channell, J.E.T., 2007, Astronomical ages for Miocene polarity chrons C4Ar–C5r (9.3–11.2 Ma), and for three excursion chrons within C5n.2n: *Earth and Planetary Science Letters*, v. 256, nos. 3–4, p. 455–465.
- Farmer, G.L., Glazner, A.F., and Manley, C.R., 2002, Did lithospheric delamination trigger late Cenozoic potassic volcanism in the southern Sierra Nevada, California?: *Geological Society of America Bulletin*, v. 114, no. 6, p. 754–768.
- Faulds, J.E., Henry, C.D., and Hinz, N.H., 2005, Kinematics of the northern Walker Lane; an incipient transform fault along the Pacific-North American Plate boundary: *Geology [Boulder]*, v. 33, no. 6, p. 505–508.
- Fisher, R.A., 1953, Dispersion on a Sphere: *Proceedings of the Royal Society of London*, v. A217, p. 295–305.
- Giusso, J.R., 1981, Preliminary geologic map of the Sonora Pass 15-minute Quadrangle, California: Reston, VA: US Geological Survey.
- Gorny, C., Busby, C., Pluhar, C.J., Hagan, J., and Putirka, K., 2009, An in-depth look at distal Sierra Nevada palaeochannel fill: drill cores through the Table Mountain Latite near Knights Ferry: *International Geology Review*, v. 51, p. 824–842.
- Hagstrum, J.T., and Gans, P.B., 1989, Paleomagnetism of the Oligocene Kalamazoo Tuff; implications for middle Tertiary extension in east central Nevada: *Journal of Geophysical Research*, v. 94, no. B2, p. 1827–1842.
- Halsey, J.H., 1953, Geology of parts of the Bridgeport, (California) and Wellington, (Nevada) quadrangles [Doctoral thesis]: Berkeley, CA, University of California, 506 p.
- House, M.A., 2001, Paleogeomorphology of the Sierra Nevada, California, from (U–Th)/He ages in apatite: *American Journal of Science*, v. 301, no. 2, p. 77–102.
- House, M.A., Wernicke, B.P., and Farley, K.A., 1998, Dating topography of the Sierra Nevada, California, using apatite (U–Th)/He ages: *Nature [London]*, v. 396, no. 6706, p. 66–69.
- Huber, N.K., 1981, Amount and timing of late Cenozoic uplift and tilt of the central Sierra Nevada, California; evidence from the upper San Joaquin River basin, US Geological Survey Professional Paper: Reston, VA: US Geological Survey, 28 p.
- Huber, N.K., 1983, Preliminary geologic map of the Dardanelles Cone Quadrangle, central Sierra Nevada, California: Reston, VA: US Geological Survey.
- Huber, N.K., 1990, The late Cenozoic evolution of the Tuolumne River, central Sierra Nevada, California: *Geological Society of America Bulletin*, v. 102, no. 1, p. 102–115.
- Huber, N.K., Bateman, P.C., and Wahrhaftig, C., 1989, Geologic map of Yosemite National Park and vicinity, California: Reston, VA: US Geological Survey.
- Jones, C.H., Farmer, G.L., and Unruh, J., 2004, Tectonics of Pliocene removal of lithosphere of the Sierra Nevada, California: *Geological Society of America Bulletin*, v. 116, nos. 11–12, p. 1408–1422.
- King, N.M., 2006, Stratigraphy, paleomagnetism, geochemistry, and anisotropy of magnetic susceptibility of the Miocene Stanislaus Group, central Sierra Nevada and Sweetwater Mountains, California and Nevada [M.S. thesis]: Sacramento, California, California State University, 81 p.
- King, N.M., Hillhouse, J.W., Gromme, S., Hausback, B.P., and Pluhar, C.J., 2007, Stratigraphy, paleomagnetism and anisotropy of magnetic susceptibility of the Miocene Stanislaus Group, central Sierra Nevada and Sweetwater Mountains, California and Nevada: *Geosphere*, v. 3, no. 6, p. 646–666.
- Kirschvink, J.L., 1980, The least-squares line and plane and the analysis of palaeomagnetic data: *Geophysical Journal of the Royal Astronomical Society*, v. 62, no. 3, p. 699–718.
- Kleinhampl, F.J., Davis, W.E., Silberman, M.L., Chesterman, C.W., Chapman, R.H., and Gray, C.H. Jr, 1975, Aeromagnetic and limited gravity studies and generalized geology of the Bodie Hills region, Nevada and California: Reston, VA: US Geological Survey, 8755–531x.

- Koerner, A., Busby, C., Putirka, K., and Pluhar, C.J., 2009, New evidence for alternating effusive and explosive eruptions from the type section of the Stanislaus Group in the 'Cataract' palaeocanyon, central Sierra Nevada, *International Geology Review*, v. 51, p. 962–985.
- Kuiper, K.F., Deino, A., Hilgen, F.J., Krijgsman, W., Renne, P.R., and Wijbrans, J.R., 2008, Synchronizing rock clocks of Earth history: *Science*, v. 320, no. 5875, p. 500–504.
- Lindgren, W., 1911, *The Tertiary gravels of the Sierra Nevada of California*: Reston, VA: US Geological Survey, 1044-9612.
- Lourens, L., Hilgen, F.J., Shackleton, N.J., Laskar, J., and Wilson, D., 2004, The Neogene period, in Gradstein, F.M., Ogg, J.G., and Smith, A.G., eds., *A geologic time scale 2004*: Cambridge: Cambridge University Press, p. 409–440.
- Manley, C.R., Glazner, A.F., and Farmer, G.L., 2000, Timing of volcanism in the Sierra Nevada of California; evidence for Pliocene delamination of the batholithic root?: *Geology [Boulder]*, v. 28, no. 9, p. 811–814.
- McFadden, P.L., and McElhinny, M.W., 1988, The combined analysis of remagnetization circles and direct observations in palaeomagnetism: *Earth and Planetary Science Letters*, v. 87, p. 161–172.
- McIntosh, W.C., 1991, Evaluation of paleomagnetism as a correlation criterion for Mogollon-Datil ignimbrites, southwestern New Mexico: *Journal of Geophysical Research*, v. 96, no. B8, p. 13,459–13,483.
- Mulch, A., Graham, S.A., and Chamberlain, C.P., 2006, Hydrogen isotopes in Eocene river gravels and paleoelevation of the Sierra Nevada: *Science*, v. 313, no. 5783, p. 87–89.
- Noble, D.C., Slemmons, D.B., Korrington, M.K., Dickinson, W.R., Al Rawi, Y., and McKee, E.H., 1974, Eureka Valley Tuff, East-Central California and Adjacent Nevada: *Geology [Boulder]*, v. 2, no. 3, p. 139–142.
- Pluhar, C.J., and Coe, R.S., 1996, Paleomagnetism of the Stanislaus Group, Table Mountain Latite Member, Sierra Nevada, California: *Eos, Transactions, American Geophysical Union*, v. 77, no. 46, p. 158.
- Priest, G.R., 1979, *Geology and geochemistry of the Little Walkr volcanic center, Mono County, California*: [Ph.D. thesis]: Corvallis, OR, Oregon State University.
- Putirka, K., and Busby, C.J., 2007, The tectonic significance of high-K₂O volcanism in the Sierra Nevada, California: *Geology [Boulder]*, v. 35, no. 10, p. 923–926.
- Ransome, F.L., 1898, *Some lava flows of the western slope of the Sierra Nevada, California*: Reston, VA: US Geological Survey, 8755-531X.
- Renne, P.R., Swisher, C.C., Deino, A.L., Karner, D.B., Owens, T.L., and DePaolo, D.J., 1998, Intercalibration of standards, absolute ages and uncertainties in (super 40) Ar/(super 39) Ar dating: *Chemical Geology*, v. 145, nos. 1–2, p. 117–152.
- Saleeby, J., and Foster, Z., 2004, Topographic response to mantle lithosphere removal in the southern Sierra Nevada region, California: *Geology [Boulder]*, v. 32, no. 3, p. 245–248.
- Saleeby, J.B., Nadin, E., Saleeby, Z., and Maheo, G., 2009, Step-over in the structure controlling the regional west tilt of the Sierra Nevada microplate: eastern escarpment system to Kern Canyon system: *International Geology Review*, v. 51, p. 634–669.
- Sharp, W., and Deino, A., 1996, CO (sub 2) laser heating of samples for (super 40) Ar/(super 39) Ar geochronology: *Eos, Transactions, American Geophysical Union*, v. 77, no. 46, p. 773.
- Slemmons, D.B., 1953, *Geology of the Sonora Pass region*: Berkeley, CA: University of California, 222 p.
- Slemmons, D.B., 1966, *Cenozoic volcanism of the central Sierra Nevada, California*: San Francisco, CA: California Division of Mines and Geology Bulletin, v. 190, p. 199–208.
- Small, E.E., and Anderson, R.S., 1995, Geomorphically driven late Cenozoic rock uplift in the Sierra Nevada, California: *Science*, v. 270, no. 5234, p. 277–280.
- Trask, J.B., 1856, *Report on the geology of northern and southern California*: State Senate Document, 66 p.
- Unruh, J.R., 1991, The uplift of the Sierra Nevada and implications for late Cenozoic epeirogeny in the western Cordillera: *Geological Society of America Bulletin*, v. 103, no. 11, p. 1395–1404.
- van Hoof, A.A.M., 1993, The Gilbert/Gauss sedimentary geomagnetic reversal record from southern Sicily: *Geophysical Research Letters*, v. 20, no. 9, p. 835–838.
- Wagner, D.L., Jennings, C.W., Bedrossian, T.L., and Bortugno, E.J., 1987, *Sacramento quadrangle map no. 1A: California Division of Mines and Geology, Regional Geological Map Series, scale 1:250,000, 4 sheets.*

- Wagner, D.L., Bortugno, E.J., and McJunkin, R.D., 1990, Geologic map of the San Francisco–San Jose quadrangle: California Division of Mines and Geology, Regional Geologic Map Series, scale 1:250,000, 5 sheets.
- Wakabayashi, J., and Sawyer, T.L., 2000, Neotectonics of the Sierra Nevada and the Sierra Nevada–Basin and Range transition, California, with field trip stop descriptions for the northeastern Sierra Nevada, *in* Brooks, E.R., and Tabilio Dida, L., eds., Field guide to the geology and tectonics of the northern Sierra Nevada: United States, State of California, Department of Conservation, Division of Mines and Geology: Sacramento, CA, p. 173–212.
- Wakabayashi, J., and Sawyer, T.L., 2001, Stream incision, tectonics, uplift, and evolution of topography of the Sierra Nevada, California: *Journal of Geology*, v. 109, no. 5, p. 539–562.
- Whitney, J.D., 1865, Report of progress and synopsis of the field work from 1860 to 1864: Geological Survey of California, v. 1, p. 243–246 (as quoted in Ransome 1898).
- Wolfe, J.A., Schorn, H.E., Forest, C.E., and Molnar, P., 1997, Paleobotanical evidence for high altitudes in Nevada during the Miocene: *Science*, v. 276, no. 5319, p. 1672–1675.
- Zijderveld, J.D.A., 1967, AF demagnetization of rocks: analysis of results, *in* Collinson, D.W., Creer, K.M., and Runcorn, S.K., eds., *Methods of Palaeomagnetism*: Amsterdam: Elsevier, p. 254–286.